JOURNAL OF AIRCRAFT
Vol. 40, No. 6, November–December 2003

Structural Response and Failure of a Full-Scale Stitched Graphite–Epoxy Wing

Dawn C. Jegley* and Harold G. Bush†
NASA Langley Research Center, Hampton, Virginia 23681
and
Andrew E. Lovejoy‡
Analytical Services and Materials, Inc., Hampton, Virginia 23666

Analytical and experimental results of the test for an all-composite full-scale wing box are presented. The wing box is representative of a section of a 220-passenger commercial transport aircraft wing box and was designed and constructed by The Boeing Company as part of the NASA Advanced Subsonics Technology program. The semispan wing was fabricated from a graphite–epoxy material system with cover panels and spars held together using Kevlar® stitches through the thickness. No mechanical fasteners were used to hold the stiffeners to the skin of the cover panels. Tests were conducted with and without low-speed impact damage, discrete source damage, and repairs. Upbending, downbending, and brake roll loading conditions were applied. The structure with nonvisible impact damage carried 97% of design ultimate load before failure through a lower cover panel access hole. Finite element and experimental results agree for the global response of the structure.

Introduction

ONE of NASA's goals is to reduce the cost of air travel by 50% in the next 20 years. To achieve this goal, NASA has been involved in the development of the technologies needed for future low-cost, lightweight composite structures for commercial transport aircraft. As a consequence of this effort, a stitched graphite–epoxy material system has been developed with the potential for reducing the weight and cost of commercial transport aircraft wing structure. By the use of stitching through the thickness of a dry graphite–epoxy material system, the labor associated with wing cover panel fabrication and assembly can be significantly reduced. By the use of stitching through the thickness of prestacked skin and then stitching together stringers, intercostals, and spar caps with the skin, the need for mechanical fasteners is almost eliminated. This manufacturing approach reduces part count and, therefore, the manufacturing cost of the structure.

To explore fully the manufacturing aspects of this new material system, a 41-ft-long wing box was fabricated by The Boeing Company as part of the NASA Advanced Subsonic Technology Program. A complete description of the wing box is presented in Ref. 1, and a summary of the NASA/Boeing program is presented in Ref. 2.

This wing box represents the load-carrying wing box of a 220-passenger commercial transport aircraft. Although originally conceived as a manufacturing development article because the stitched, resin-film-infusion (RFI) process had never been used on a composite structure of this size and complexity, the wing was designed to withstand loads associated with several flight conditions. The most critical loading conditions examined were -1-g downbending, 2.5-g upbending, and a brake roll runway condition where twist is applied through the simulated landing gear leg. The wing box was loaded in a series of tests covering all three load conditions and then loaded to failure at the NASA Langley Research Center. Included in the test series were tests to evaluate the behavior of the wing box when subjected to nonvisible impact damage, discrete source damage, and repair. A photograph of the wing before testing is shown in Fig. 1. Nine load introduction locations are shown in the Fig. 1, and load was applied by pushing up on the wing or pulling down on the wing, depending on the load case. The present paper focuses on the final loading of the test article in the 2.5-g upbending condition.

Wing-Box Test–Specimen Description

The wing-box cover panels and spars were fabricated from stitched/resin-film-infused graphite–epoxy material, minimizing the number of mechanical fasteners needed to assemble the wing box. The composite upper cover skin and upper cover blade stiffeners were composed of layers of graphite material forms that were prekitted in nine-ply stacks using Hercules, Inc., AS4 fibers. Each nine-ply stack had a $[45/-45/0_2/90/0_2/-45/45]_T$ laminate stacking sequence and was approximately 0.055 in. thick. The composite lower cover panel skin was composed of 0-deg layers of Hercules, Inc., IM7 fibers and ± 45- and 90-deg layers made from AS4 fibers. Prekitted stacks were assembled in a similar manner as for the upper cover panel skin. Several stacks of the prekitted material were used to build up the desired thickness at each location. Skin thickness ranged from 0.265 to 0.605 in. Upper cover stringer blades ranged in thickness from 0.44 to 0.605 in. Braided stringers, as described in Ref. 1, of AS4 fibers were used in the lower cover panel. Braided stringer blades ranged in thickness from 0.48 to 0.768 in. and contain ± 60-deg braids. All material was stitched together using E. I. DuPont de Nemours, Inc., Kevlar® thread. Stiffener flanges for stringers in the spanwise direction, intercostals in the chordwise direction, and spar caps along the forward and aft edges of the cover panels were stitched to the skin, and no mechanical fasteners were used for joining. The composite wing box was fabricated using Hercules, Inc., 3501-6 epoxy in an RFI process, which is described in Refs. 3 and 4. Stitched graphite–epoxy spars with the same stacking sequence and material as the upper cover panel skin were mechanically attached to the spar caps. Tape-laid graphite–epoxy ribs were mechanically fastened to the intercostals to create the 41-ft-long wing box. The wing box measured approximately 8 by 3 ft at the root end and 4 by 2 ft at the tip. The upper and lower cover panels are shown in Figs. 2a and 2b, respectively. In Fig. 2, 18 ribs and 10 stringers are identified by number. Holes are identified by hole number starting with the most inboard hole.

Presented as Paper 2001-1334 at the AIAA/ASME/ASCE/AHS 42nd Structures, Structural Dynamics, and Materials Conference, Seattle, WA, 16–19 April 2001; received 6 March 2002; revision received 10 November 2002; accepted for publication 10 November 2002.

*Senior Aerospace Engineer, Mechanics and Durability Branch. Senior Member AIAA.
†Senior Aerospace Engineer, Mechanics and Durability Branch. Associate Fellow AIAA.
‡Senior Aerospace Engineer. Senior Member AIAA.

Fig. 1 Test article before testing.

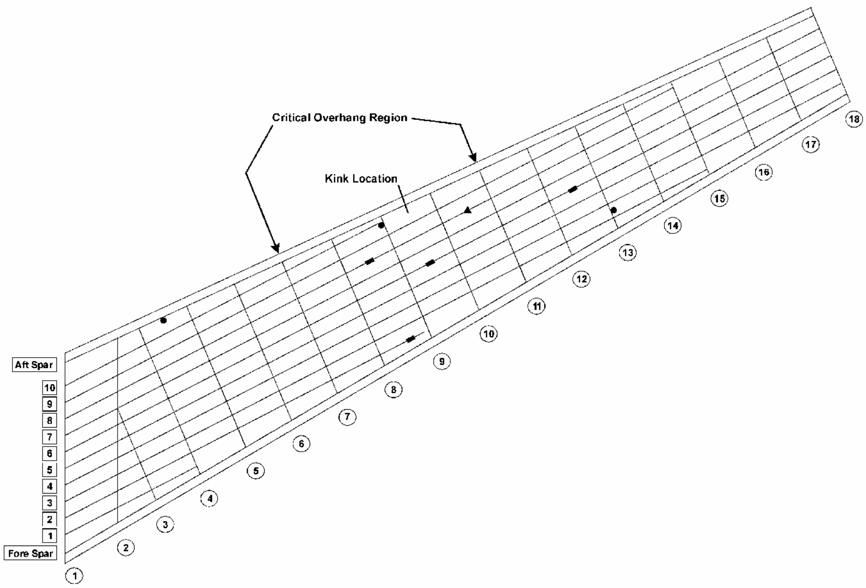

a) Upper cover panel

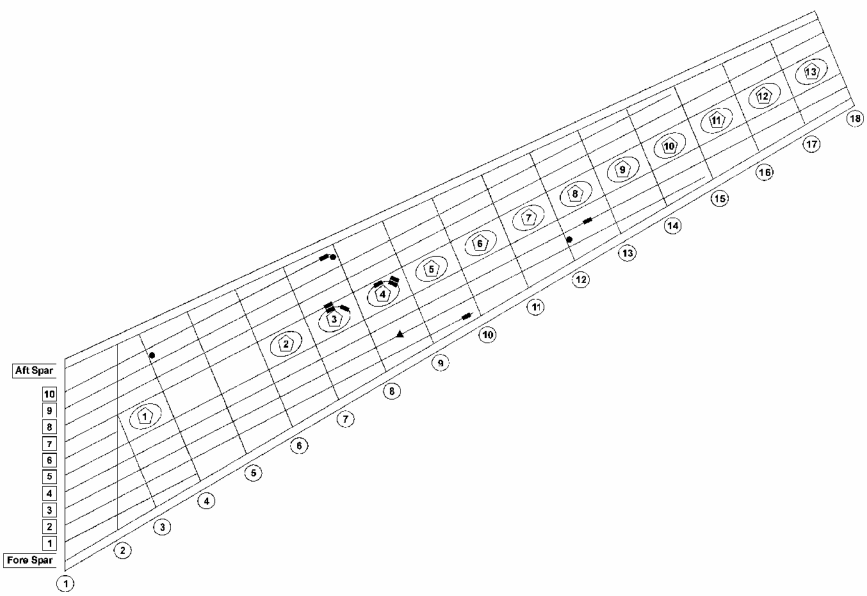

b) Lower cover panel

Fig. 2 Upper and lower panel configuration and strain gauge locations: ○, rib number; □, stringer number; ⌂, hole number; ▲, sawcut/repair; ●, impact damage; and ■, strain gauge locations.

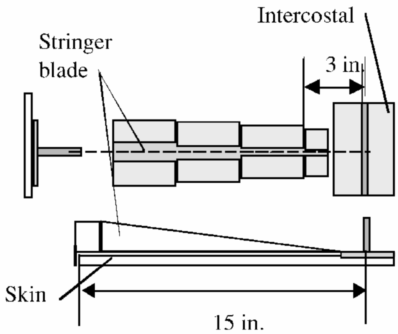

a) Tapered-height stringer runout

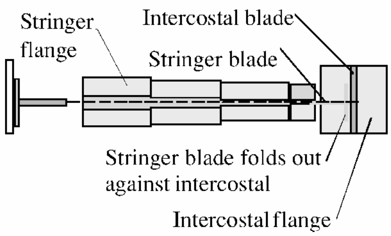

b) Constant-height stringer runout

Fig. 3 Stringer termination configurations.

The upper and lower cover panels each contain five stringer terminations or runouts. Blade and flange thicknesses are reduced by removing two stacks of material at a time, at 3-in. intervals in all runouts. Lower cover stringers terminating at ribs 8, 10, and 15 and the upper cover stringers terminating at rib 9 have a tapered height blade, as shown in Fig. 3a. The lower cover stringer terminating at rib 4 and the upper cover stringers terminating at ribs 4 and 15 have a constant height blade and terminate by folding the last two stacks of stringer material against the intercostal, as shown in Fig. 3b. The upper cover panel blade height is tapered from a maximum of between 2.5 and 3.25 in. to 0 at a taper angle of 8 deg. The lower cover panel blade height is tapered from a maximum of between 2.65 and 3.5 in. to 0 at a taper angle of 11 deg.

Finally, load-introduction hardware was attached to the wing box before shipment to NASA Langley Research Center. The load-introduction hardware included fixtures at each of the actuator attachment locations, metal landing gear doublers on the upper and lower cover panels, and a root mount transition box that provided a method of attaching the wing box to the load wall in the test facility. On installation at the test facility, a simulated landing gear leg was attached to the doubler assembly through the use of two 9-in.-diam steel bolts.

Mounting and Loading Apparatus

Each actuator/load cell assembly 1–9 was connected to the floor and to the test article through swivels that would allow the actuator to rotate as the wing box deformed. This rotation prevented the introduction of localized bending loads into the wing lower surface at load introduction points 1–8 shown in Fig. 1. The loading assembly for a typical actuator is shown in Fig. 4. The landing gear region includes three actuator assemblies as described in detail in Ref. 5 but are not described herein because only vertical actuators were active during the 2.5-*g* loading tests.

Loading Sequence

The wing structure was subjected to eight tests with three load conditions as listed in Table 1. These conditions are brake roll, −1 and 2.5 *g*. The brake roll load condition simulates a runway condition in which forces are applied primarily through the landing gear leg. The −1 and 2.5 *g* load conditions simulate extreme flight loading conditions. In the test, the wing tip is pulled down to simulate a −1-*g* flight maneuver and pushed up to simulate a 2.5-*g* flight maneuver. The values of load at design limit load (DLL) for each

Table 1 Test sequence

Test number	Loading condition
1	50% DLL, brake roll
2	100% DLL, brake roll
3	50% DLL, −1 *g*
4	50% DLL, 2.5 *g*
5	100% DLL, −1 *g*
6	100% DLL, 2.5 *g*
7	70% DLL, 2.5 *g*
8	Failure/150%DLL, 2.5 *g*

Table 2 DLL values for three load conditions

Actuator position[a]	Brake roll,[b] lb	−1 *g*,[b] lb	2.5 *g*,[b] lb
1	−1,000	−6,000	27,000
2	−2,000	−30,000	66,500
3	−1,000	−22,000	−2,000
4	−2,000	8,000	14,000
5	−8,000	−6,000	10,000
6	−11,500	11,500	−30,000
7	0	−3,000	30,000
8	10,000	−9,500	4,000
9	124,450	0	0

[a]Shown in Fig. 1.
[b]Positive load is due to pushing up and negative load is due to pulling down.

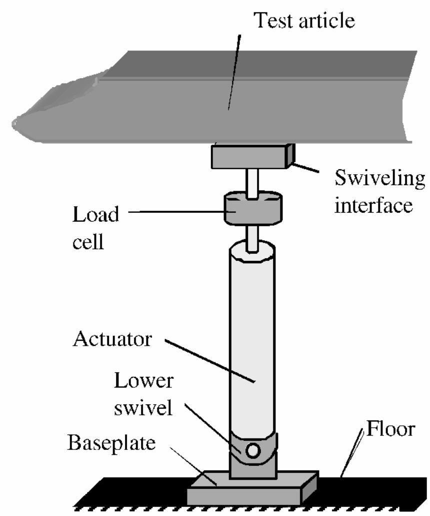

Fig. 4 Actuator/load cell assembly.

of these load conditions are shown in Table 2 for all of the load introduction points. Positive values in Table 2 refer to pushing up on the wing and negative values refer to pulling down on the wing. Because these values simulate flight conditions, a combination of pushing up and pulling down is required in each load condition to achieve the desired wing motion.

First the test article was subjected to two brake roll tests: a 50% DLL test to verify accurate function of all components and instrumentation, followed by a 100% DLL test. Then two more 50% DLL loadings were conducted to verify the accurate function of all components and instrumentation for the −1- and the 2.5-*g* flight loading conditions. The wing was then loaded to 100% DLL in these two conditions.

After successful completion of all 100% DLL tests, discrete source damage was inflicted on the upper and lower cover panels of the wing. The wing was then loaded to 70% DLL in the 2.5-*g* upbending condition and unloaded. Finally, the discrete source damage was repaired, six nonvisible impacts were inflicted, and the wing was loaded to failure in the 2.5-*g* upbending load condition.

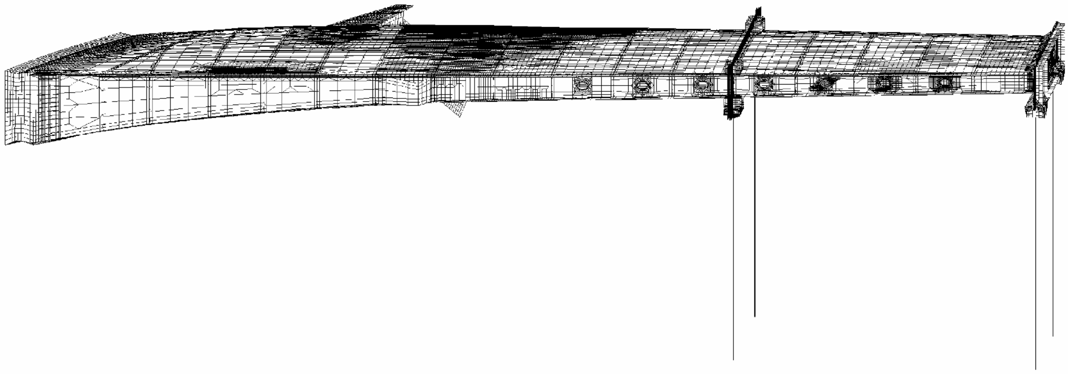

Fig. 5 Finite element model of test article.

Instrumentation and Control

A computer control system and an independent computer data acquisition system were used during testing. Loading was increased slowly to a maximum with all actuators reaching the maximum loading simultaneously. Load rates varied among the different tests, but generally tests were planned to run for 15–30 min. Feedback signals were sent to the control system to keep the actuators loading evenly throughout each test. Data were recorded at the rate of once every second as load was applied during each test.

Displacements were measured using displacement transducers at each actuator location and at the two points on the lower surface where the root transition box connected to the composite box at the front and rear spar. All over the test article, 466 strain gauges were used to record strains. Locations of critical strain gauges for the upper and lower cover panels are shown in Fig. 2. Strain gauges shown at the access holes are on the edge of the hole at the midplane, not on the cover panel surface. All other gauges were placed on the skin or stringer blade surface.

Impact, Discrete Source Damage, and Repair

Impact damage was inflicted by the use of a dropped-weight and air-propelled projectiles. Impact damage was inflicted to the upper and lower surfaces of the wing. Details of these damages are presented in Ref. 6. A dropped-weight impactor was used to inflict three impacts with an energy level of 100 ft · lb to the upper cover panel. The locations of these damage sites are shown in Fig. 2a. A weight of 25 lb with a 1-in.-diam tup was dropped vertically from 4 ft, resulting in barely visible damage. The depth of the resulting damage ranged from 0.01 to 0.05 in.

An air-propelled steel projectile was used to inflict three impacts with an energy level of 83–84 ft · lb to the lower cover panel. The locations of these damage sites are shown in Fig. 2b. A steel sphere with a 0.5 in. diameter was accelerated to a speed of approximately 545 ft/s, resulting in clearly visible damage with dent depths up to 0.135 in.

The wing was subjected to discrete source damage in the form of 7-in.-long sawcuts to the upper and lower cover panels, as shown in Fig. 2. Each sawcut ran through two stinger bays and cut through a stringer. Metal patch repairs were used to restore the wing to full load-carrying capability. The damaged region was removed before implementing the repair. The repairs consisted of a metal plate that conformed to the wing surface on the outer surface of the cover panels and internally spliced stringers. All parts of the repair were attached to the wing with mechanical fasteners.

Finite Element Analysis

A finite element analysis of the entire test article was conducted using the finite element code STAGS.[6] The analysis accounts for geometric nonlinearities but not plasticity. Several versions of the finite element model were constructed, each with refined regions in the part of the structure of interest for a particular loading condition. Results for several of these models are presented in Ref. 7 covering studies conducted before testing. Only results from the post-test analysis of the 2.5-g failure test, not presented in Ref. 7, are presented herein.

All critical structural components are modeled using shell elements, including cover panels, spars, ribs stringers, root mounting fixture, and load introduction fixtures for actuators 1–4. The load fixture for actuator 5 is modeled using offset beam elements. Beam elements are also used to model spar and web stiffeners, intercostals, bolts, and actuators 1–4. The stringer runouts are modeled in detail to represent accurately the taper in height and stack drop offs. This detail is necessary to capture the local behavior in the region of the runouts. The finite element model for posttest analysis is shown in Fig. 5, which has approximately 71,000 nodes and 76,000 elements, for a total of approximately 428,000 degrees of freedom.

Because of the large deformations that occur on the outboard portion of the test article and the possible effects of load orientation on the load fixture response, actuators 1–4 are included in the model. These actuators are represented by beams having no axial stiffness and high bending stiffness. The load (shown in Table 2) for each actuator is then applied to the actuator beam end and is treated as a follower force with respect to the actuator beam during the nonlinear analysis. The base of the actuator beam is fixed in space at the floor location by setting all three translations of the base node equal to zero. The rotation about the global y axis is also set to zero to prevent rigid-body motion. Proper orientation of the follower loads is ensured by requiring appropriate compatibility at the connection between the actuator beam and its load introduction fixture. This technique is discussed in detail in Ref. 7.

Post-test analysis is primarily concerned with understanding the behavior observed during the final test. Therefore, because the observed failure and measured nonlinearities occurred between ribs 8 and 9, the model was highly refined between ribs 7 and 11 only.

Results and Discussion

Results are shown for the final test under the 2.5-g load condition only, test 8. Analytical results for the undamaged test article subjected to brake roll and −1-g conditions and the sawcut test article loaded in the 2.5-g condition are presented in Ref. 7. Experimental results for tests in all three load conditions and with impact and discrete source damage are presented in Ref. 5. No evidence of damage to the structure was detected in tests 1–7. Analytical and experimental results for the final test are presented herein.

The test article supported 97% of its design ultimate load (DUL) before failure in test 8. DUL is 150% of DLL. A photograph of the test article loaded at 95% DUL is shown in Fig. 6.

Displacement

Analytical and experimental displacements at the six most outboard actuator locations are shown in Fig. 7. Solid lines represent the measured displacements and dashed lines represent predicted displacements. Measured displacements are the elongation of the actuator rather than a measurement perpendicular to the floor. Because the initial position of all actuators active in the 2.5-g condition is vertical, the difference between the displacement perpendicular to

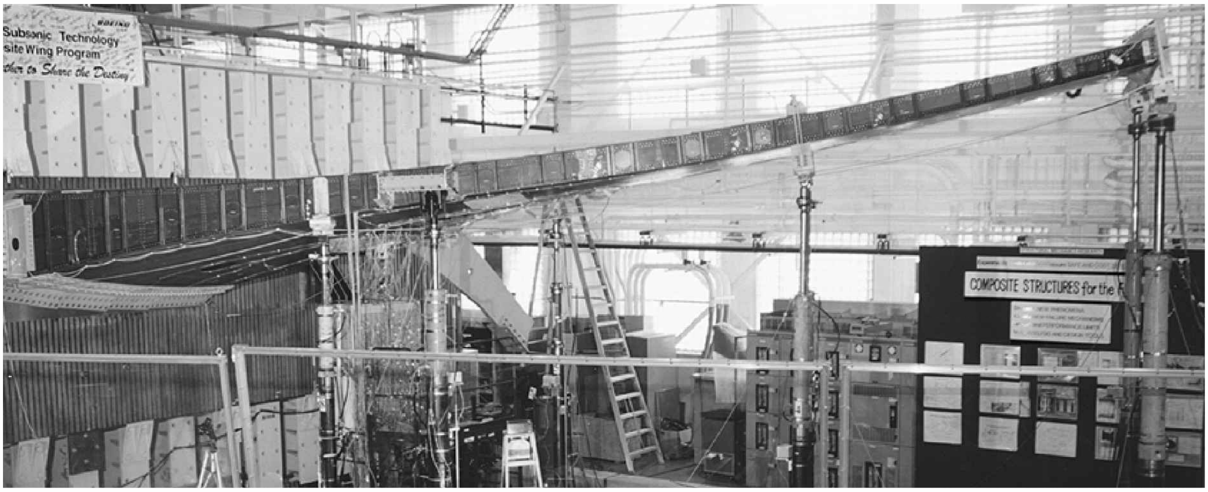

Fig. 6 Deformed test article loaded to 95% of DUL.

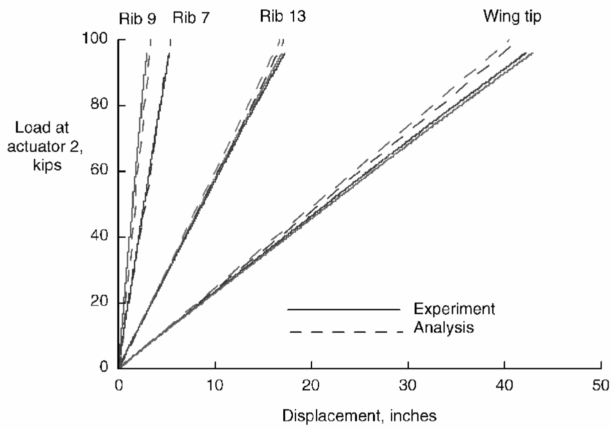

Fig. 7 Displacements at six outboard load introduction points (1 kip = 1000 lb).

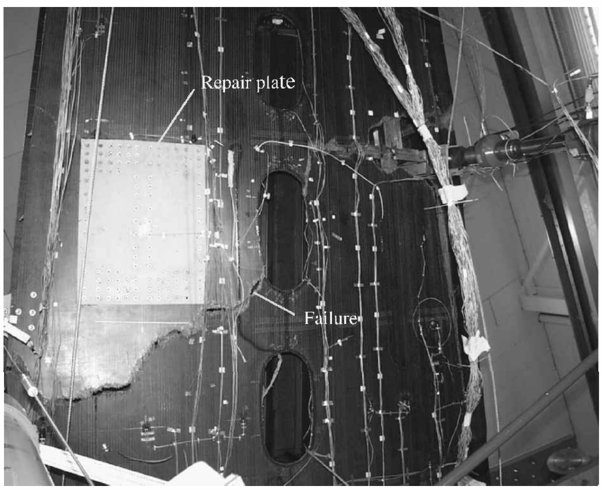

Fig. 8 Failure across lower cover panel.

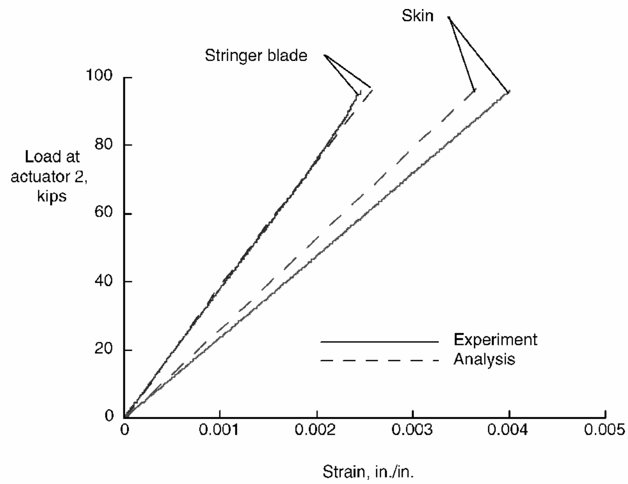

Fig. 9 Strain in stringer blade and skin at stringer 4 in the lower cover panel between ribs 12 and 13.

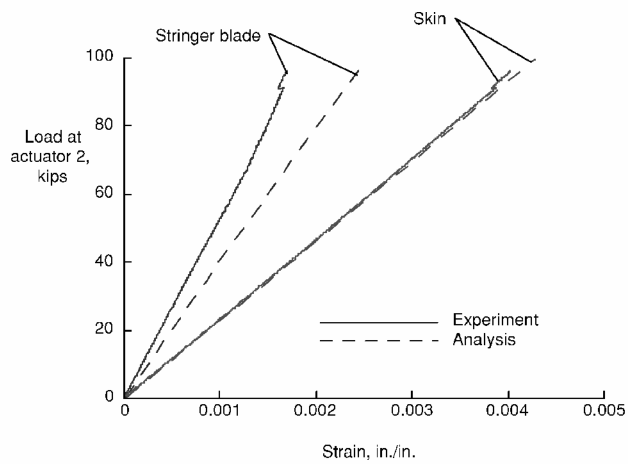

Fig. 10 Strain in stringer blade and skin at stringer 7 in the lower cover panel between ribs 7 and 8.

the floor and the stroke of the actuator is dependent on the rotation of the actuator during loading. The largest displacement (and largest rotation) is for actuator 2 at the wing tip. The measured deflection is 40 in., and the initial position of the intersection of the actuator assembly and the test article is 168 in. above the floor. The angle between the initial vertical position of the actuator and the final tilted position can be calculated to be less than 2 deg, resulting in a negligible difference between vertical displacement and stroke.[7] Analytical results for the global displacements are within 8% of the experimental results for the final test.

Strain

The primary failure location is across the lower cover panel through access hole 4. This region of the lower cover panel after final failure is shown in Fig. 8. The failure goes through all stringers but primarily remains between ribs 8 and 9. Both spars were also damaged. Other minor damage was found but appears to be unrelated to the initial failure event. The discussion of the failure will be limited to the regions between ribs 6 and 10.

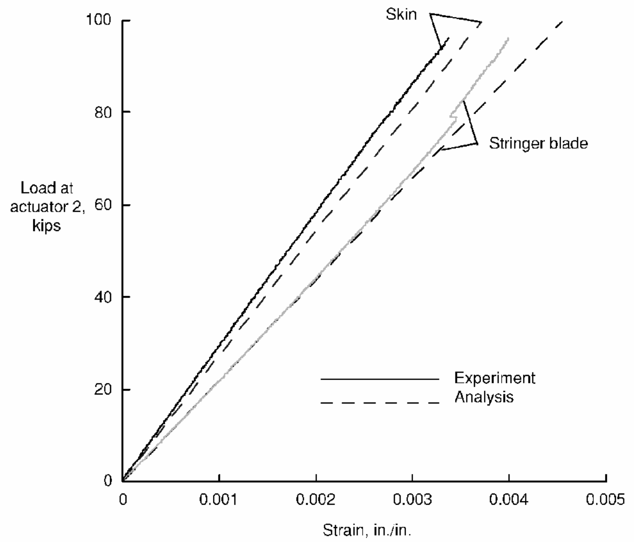

Fig. 11 Strain in stringer blade and skin at stringer 2 in the lower cover panel between ribs 9 and 10.

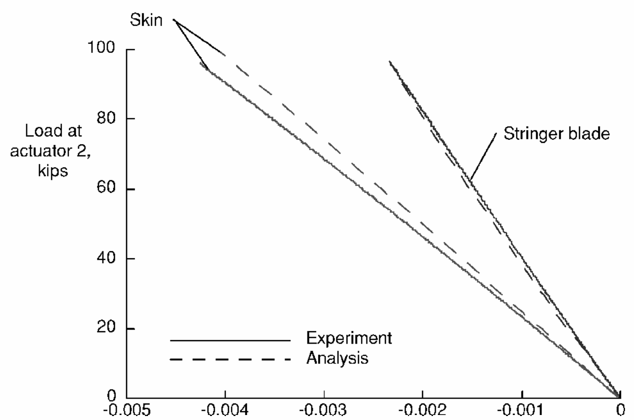

Fig. 12 Strain in stringer blade and skin at stringer 6 in the upper cover panel between ribs 12 and 13.

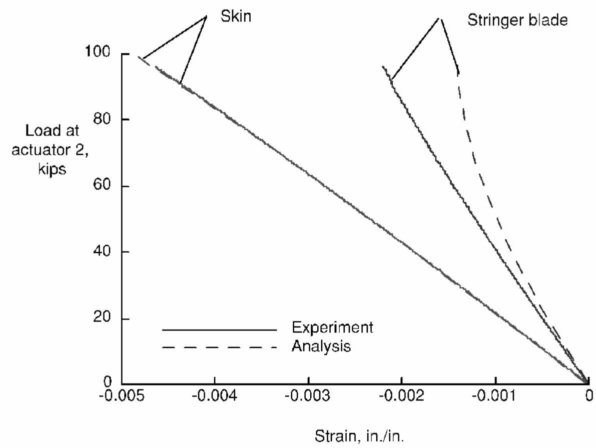

Fig. 13 Strain in stringer blade and skin at stringer 6 in the upper cover panel between ribs 9 and 10.

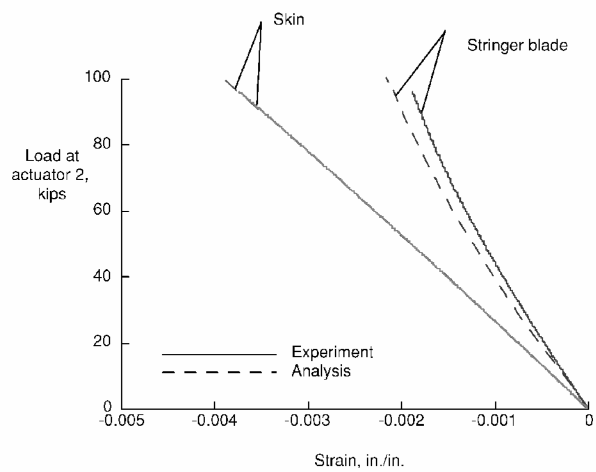

Fig. 14 Strain in stringer blade and skin at stringer 2 in the upper cover panel between ribs 8 and 9.

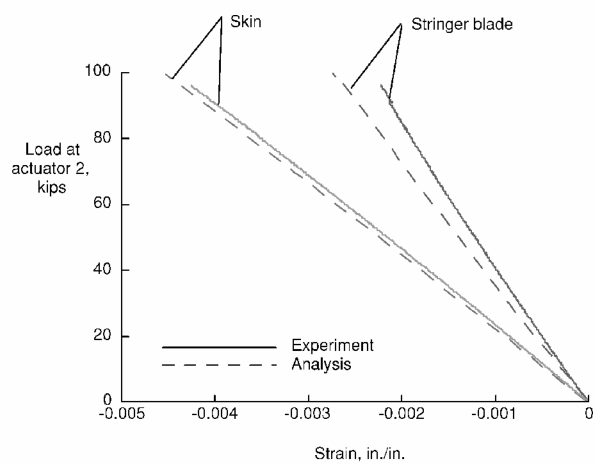

Fig. 15 Strain in stringer blade and skin at stringer 8 in the upper cover panel between ribs 8 and 9.

Strain results presented herein follow a convention that negative values are compressive and positive values are tensile. All strain results are plotted against the load in actuator 2. Upper cover panel and lower cover panel strains are presented. Locations of the strain gauges of interest are shown in Fig. 2. Back-to-back gauges were placed on the outer surface of the cover panel skin and either the cover panel skin inner surface or the top of the stringer blade. Representative strain gauge results are shown in Figs. 9–15. In strain result Figs. 9–15, solid lines represent measured strains and dashed lines represent analytical results.

Strains in the lower cover panel at stringer 4 between ribs 12 and 13 and at stringer 7 between ribs 7 and 8 are shown in Figs. 9 and 10, respectively. Excellent correlation between experiment and analysis is seen in the skin between ribs 7 and 8 and in the stringer between ribs 12 and 13 until immediately before failure. The repair, which was not modeled in the analysis, is located between ribs 8 and 9 and may have some influence on these blade strains. Strains remain linear until immediately before failure. Strains in the lower cover runout of stringer 2 where it terminates at rib 10 are shown in Fig. 11. Analytical strains at this runout agree well with experimental data.

Strains in the upper cover panel at stringer 6 between ribs 12 and 13, at stringer 6 between ribs 9 and 10, at stringer 2 between ribs 8 and 9, and at stringer 8 between ribs 8 and 9 are shown in Figs. 12, 13, 14, and 15, respectively. For most of these cases, the agreement between analytical and experimental results is good. Excellent correlation between experiment and analysis is seen in the skin inboard from rib 12 and in the stringer outboard from rib 12 until immediately before failure. The repair, which was not modeled, is located between ribs 10 and 11 and may have some influence on experimental strain data. Strains do not remain linear in the upper cover panel. The maximum strains in any upper cover runout location are in the runout region at the rear spar at rib 9. Strains at this stringer runout 10.5 in. inboard from rib 9 are shown in Fig. 14. The blade is tapered in height as well as thickness at this location.

An overhang of the cover panels with a width of approximately 4 in. behind the rear spar left an unsupported edge along the length of the test article. This region is shown in Fig. 2a as the critical overhang region. A small initial geometric imperfection in the form of a kink in the upper cover panel was present in the as-manufactured

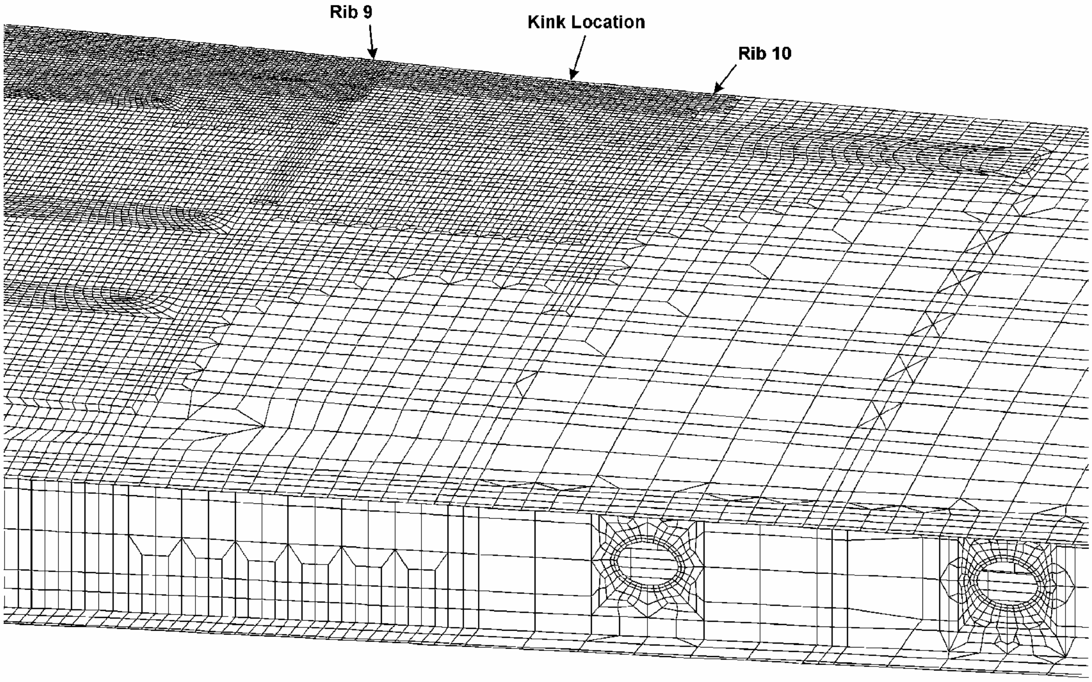

Fig. 16 Finite element model of kink region.

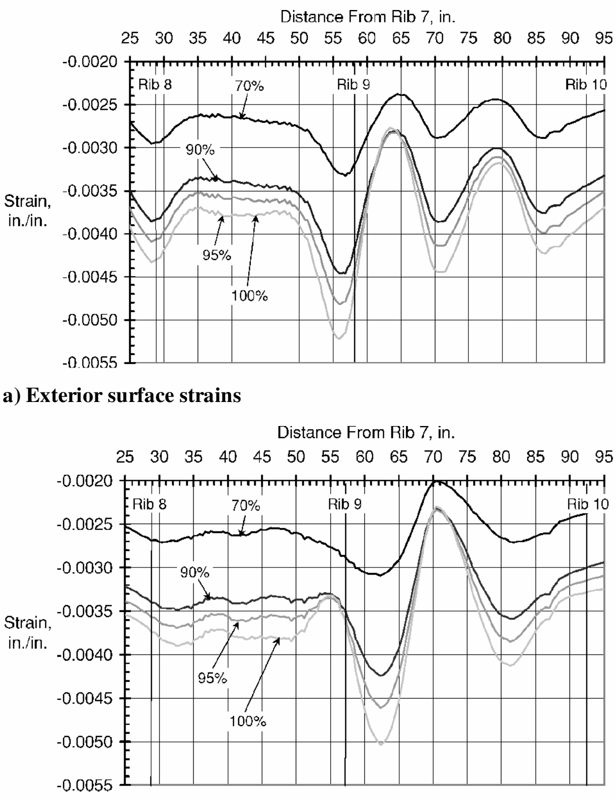

a) Exterior surface strains

b) Interior surface strains

Fig. 17 Strains in the upper cover overhang region aft edge at several values of percent DUL.

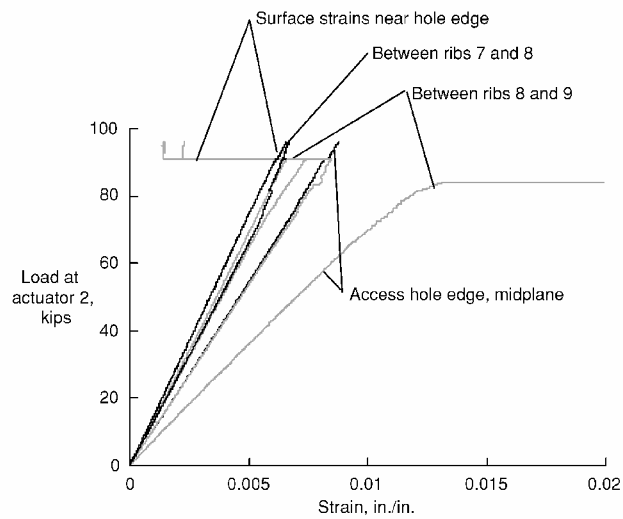

Fig. 18 Measured strain results at the edge of critical access holes.

structure. This kink is centered half way between ribs 9 and 10 and has a maximum depth of 0.1 in. The kink was initially considered minor enough that it would not influence the cover panel structural behavior. However, because the kink is in close proximity to a stringer runout and is in the region of the upper cover panel that displays nonlinear behavior, the kink influenced the behavior of the overhang region. Therefore, the kink was included in the posttest finite element model. This local refinement is shown in Fig. 16. The kink is a geometric imperfection in the skin.

Calculated strains along the rear overhang of the upper cover for the outer and inner skin surfaces for load levels of 70, 90, 95, and 100% DUL are shown in Fig. 17. Reversal of strain occurs in several places along the exterior cover surface. Strain reversal for the outer skin surface occurs 6–8 in. outboard of rib 9. Strain reversal for the inner skin surface occurs from 1 to 4 in. inboard of rib 9 and from 13 to 15 in. outboard of rib 9. There were very few strain gauges in this region, and hence, experimental results are not presented.

Strain gauges at the edges of the lower cover panel access holes indicate high strains at these locations. Measured strains at the outboard, rear corner of access holes 3 and 4, between ribs 7 and 8 and ribs 8 and 9, respectively, are presented in Fig. 18. The strain gauge locations are shown in Fig. 2b. Nonlinearity in the load-strain behavior can be seen at these access holes. The most significant nonlinearity is at the outboard corner of access hole 4. The largest measured strain is at this location and is approximately 0.0096 in./in. at DLL. Final failure of the cover panel ran through this location. Because analytical results to date do not adequately capture the failure, comparisons of these strains for the access hole edges are not done with experimental results.

Summary

A 41-ft-long graphite–epoxy stitched wing box was tested in three load conditions and ultimately to failure. The test article is representative of a section of a 220-passenger commercial transport wing. The structure was fabricated using advanced manufacturing techniques to reduce cost and weight and to improve damage tolerance capability. The test article sustained 97% of DUL before failure through a lower cover access hole that resulted in the loss of the entire lower cover panel. In addition to the high strains at the lower cover panel access holes, strain gauge results indicate that local nonlinear deformations occurred in the upper cover panel in an unsupported region behind the rear spar. Experimental and analytical results are in good agreement for global behavior. Larger local displacements and strains occurred in the test than are predicted in the nonlinear finite element analysis. Further refinements to the finite element model might provide a better agreement of the analytical results with the test data.

Acknowledgments

The authors wish to express their thanks to William R. Doggett, William S. Small, and Cheri L. Bailey of NASA Langley Research Center and Byron L. Stonecypher of Wyle Laboratories for their support in the testing of the stitched semispan wing.

References

[1]Hawley, A., "Preliminary Design of a Transport Aircraft Composite Wing," *Proceedings of the Fifth NASA/DoD Advanced Composites Technology Conference*, NASA CP-3294, Vol. 1, Pt. 2, 1994, pp. 717–772.

[2]Karal, M., "AST Composite Wing Program—Executive Summary," NASA CR-2001-210650, Aug. 2001.

[3]Markus, A., Thrash, P., and Grossheim, B., "Manufacturing Development and Requirements for Stitched/RTM Wing Structure," *Proceedings of the 4th NASA/DOD Advanced Composites Technology Conference*, NASA CP-3229, 1993, pp. 503–523.

[4]Rohwer, K., Ghumman, A., and Markus, A., "Stitched/Resin Film Infusion (S/RFI) Manufacturing Technology Development," *Proceedings of the 11th DOD/NASA/FAA Conference on Fibrous Composites in Structural Design*, pp. XIII-93–116.

[5]Jegley, D. C., and Bush, H. G., "Structural Testing of a Stitched/Resin Film Infused Graphite–Epoxy Wing Box," NASA TM-2001-210846, April 2001.

[6]Rankin, C. C., Brogan, F. A., Loden, W. A., and Cabiness, H. D., "STAGS User Manual, Version 3.0," Lockheed Martin Missiles and Space Co., Palo Alto, CA, March 1999.

[7]Lovejoy, A. E., "Finite Element Analysis of a Composite Semi-Span Test Article with and Without Discrete Damage," NASA CR 2000-210308, Aug. 2000.